Parasitics of Orthocyclic Windings in Inductors and Transformers

Shen, Zhan; Wang, Huai

Published in:
I E E E Transactions on Power Electronics

DOI (link to publication from Publisher):
10.1109/TPEL.2020.3006882

Publication date:
2021

Document Version
Accepted author manuscript, peer reviewed version

Parasitics of Orthocyclic Windings in Inductors and Transformers

Zhan Shen, *Student Member*, and Huai Wang, *Senior Member*

***Abstract*— The orthocyclic winding in magnetic components is common in both laboratory prototyping and mass-production, especially for round wires with curved edges. However, its impact on winding parasitics, i.e., the winding capacitance, ac resistance, and leakage inductance, has not been systematically investigated. Omission or inaccurate calculation of those parameters lead to current ringing, additional losses, and even abnormal operations. In this paper, three modified formulas for parasitics of orthocyclic windings are proposed, and the impacts of the orthocyclic windings are comprehensively studied. The magnetic field distortion and air-gap effect are analyzed and compensated. The formulas are verified by finite element method (FEM) simulation and experimental results. Finally, a comparison of the normal and orthocyclic winding is performed, and conclusions are listed to control the parasitics of orthocyclic windings.**

***Index Terms*—Orthocyclic winding, stray capacitance, ac resistance, leakage inductance, inductor, transformer.**

I. Introduction

The parasitic parameters of magnetics, i.e., the ac resistance, leakage inductance, and stray capacitance, have significant impacts on the circuit performance [1, 2]. Typical parasitic models of the inductor and transformer are in Fig. 1(a) and (b). For the inductor, L is the inductance, $C_{\rm ind}$ is the stray capacitance, $R_{\rm p}$ and $R_{\rm w}$ are the equivalent core and winding resistance, respectively. For the transformer, R_1, $L_{1\sigma}$, C_1 and R_2, $L_{2\sigma}$, C_2 are the resistance, leakage inductance, and inner-winding capacitance of the primary and secondary, respectively, and C_{12} is the inter-winding capacitance. Minimizing the ac resistance decreases the resistive loss and increases the efficiency of magnetics [3, 4]. A certain value of the transformer leakage inductance is required for the power transferring and current shaping in the dual active bridge converter [5, 6], while in other cases it may need to be minimized [7]. Stray capacitance causes severe current ringings and capacitive switching losses [8, 9].

Those parasitics highly depend on winding configurations, as illustrated in Fig. 1(c). The current flows in the windings and induces the magnetic field. As the increase of frequency, there are eddy currents in wires, which generate resistive losses in the winding. Those losses are represented by the ac resistance, i.e., winding resistance of inductors $R_{\rm w}$, pri-

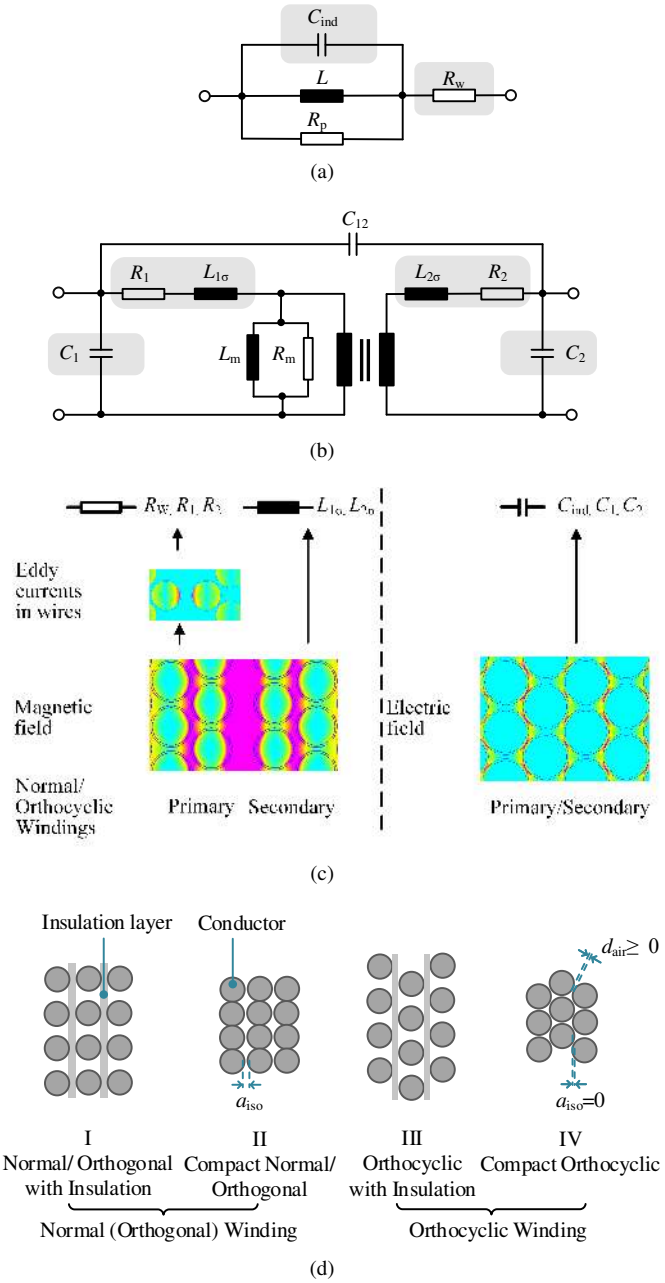

Fig. 1. The parasitic model of magnetics. (a) Inductor circuit model. (b) Transformer circuit model. Winding parasitics discussed in this paper is highlighted in gray in (a) and (b). (c) From magnetic/ electric field to winding parasitics. (d) Four typical winding positions. $d_{\rm air}$ is the width of air gap. $a_{\rm iso}$ is the inter-layer insulation distance.

Zhan Shen and Huai Wang are with the Center of Reliable Power Electronics (CORPE), Department of Energy Technology, Aalborg University, Aalborg 9220, Denmark (e-mail: zhs@et.aau.dk and hwa@et.aau.dk).

mary and secondary resistance of transformers R_1, R_2. The magnetic field in the transformer also stores the magnetic energy in the winding area, which is represented by the leakage inductance $L_{1\sigma}$ and $L_{2\sigma}$. Moreover, the voltage applied on the winding generates the electric field between each turn, so the winding also stores the electric field energy as a capacitor. This capability is represented by stray capacitances, i.e., winding capacitance of inductors C_{ind}, primary and secondary winding capacitance C_1 and C_2. The variation of winding configurations also affects those parasitic values. So proper magnetic and electric field models based on a precise winding configuration are essential.

Usually the windings are designed and modeled as the normal configuration, i.e., type I & II in Fig. 1(d). However, for round wire windings, they displace from the normal position and become type III and IV. This is due to the curved edge and unstable shape of the wire, and is normal in high-turn-ratio and high-voltage windings. Winding IV without insulation layer is also used to reduce the cost and increase window utilization factor. Normally a tolerant error is used to explain the difference between the normal and orthocyclic windings. However, in some scenarios, even a slight displacement causes a significant variation of parasitics, e.g., stray capacitance values. So the orthocyclic position should be considered in the parasitic modeling. The major research of the winding parasitics focuses only on normal windings. They are briefly reviewed below.

The classic formula for the winding ac resistance is proposed by Dowell [10] and is widely applied for ac resistance optimization [11–13]. It is derived in the Cartesian coordinate system, and assumes that the magnetic flux is parallel to the winding in height direction. However, the flux can distort in two or three dimensional as the changing of the porosity factor, conductor shape, etc. So the assumption becomes weak and the accuracy decreases [14, 15]. There are mature models to compensate the field distortion by modifying Dowell's equation. Firstly, when the porosity factor η, i.e., the winding height divided by the core window height, decreases, there is magnetic field distortion. Analytical models in [16, 17] use η as the adjust coefficient in to compensate this effect, while models in [18, 19] solve the two-dimensional field directly. Secondly, the winding curvature also leads to the two dimensional effect, and the analytical solution in the cylindrical coordinates is used to modify Dowell's equation with correction factors [20]. Thirdly, the analytical model is also improved by coefficients considering the thermal effect [21], asymmetric coupling [22], phase shift between winding currents [23], etc. For the Litz wire, there are analytical models derived from both Cartesian and cylindirical coordinates systems [4, 24, 25]. Moreover, the Finite Element Method (FEM) is with significant improvement of accuracy by considering the two or three dimensional field distribution in the simulation. Adopting it for the fast resistance calculation [26, 27] or using the simulation results to fit corresponding analytical formula coefficients offline [28–30], those models achieve good accuracy without too much calculation burden. Finally, the orthocyclic winding also distorts the magnetic field and has two dimensional effect. However, a discussion about its impact is still missing.

The leakage inductance is induced by the same magnetic field as the ac resistance. Most analytical methods are based on the magnetic field analysis, stored energy integration, and then leakage inductance calculation. The leakage inductance formula is also given in Dowell's paper [10]. Different from the low-frequency leakage inductance model [31], Dowell's model considers the high-frequency magnetic field and eddy current distribution [32]. By combing the result of the energy storage in the windings in [10] and in the isolation and insulation layers in [31], a practical formula is proposed in [33]. A recent advance in [6] proposes an expression through a detailed analysis of the energy stored in each winding part. Besides, there are also leakage inductance models for other different winding types, e.g., Litz wire windings [34], planar transformers windings [32, 35, 36], windings with magnetic shunt [37], coaxial coils in air [38], asymmetric parallel windings [39], transformers with gaped cores [40–42], and windings around toroidal cores [43, 44]. Different winding configurations are compared in [45] and their impact to the leakage inductance is analyzed. Moreover, there are also investigations on the impact of the field distortion to the leakage inductance. Dowell's model assumes a straight field line along the winding. However, this assumption becomes week when the porosity factor η decreases, or the turns of the winding displaces. [46] derives the field distortion around the winding analytically. By solving the field, the proposed semi-analytical model achieves comparable accurate results than the FEM simulation. [47] also observes the uneven geometric magnetic field distribution, and uses a correction factor in the analytical model to modify the equivalent height of the winding. For the orthocyclic winding, in [48, 49], the probabilistic distribution of the leakage inductance of transformers with non-ideal winding is obtained. All types of windings with not ordered turns, including orthocyclic windings, are considered. For orthocyclic winding type IV, the inter-layer insulation distance a_{iso} in formulas are zero or even may be negative, as in Fig. 1(d). The inter-layer energy is then underestimated, which does not coincide with the field distribution in reality. Therefore a new leakage inductance formula is needed.

The stray capacitance of magnetics consists the winding capacitance and the capacitance between the winding and core, i.e., core-related capacitance. The FEM electrical field simulation obtains the winding capacitance considering the impact of the core and the field distortion. It is used to model the normal winding capacitance in two dimensional [50] or three dimensional filed [51]. A hybrid method is proposed in [52] to use the results from analytical calculation for the fast simulation. The model in [53] uses a set of simulation results to fit coefficients in analytical models, which obtains precise winding capacitance of single layer winding and can be extend for multi-layer windings. For the analytical models, various formulas are reviewed in [1]. The core-related capacitance models are proposed in [54–59]. For the winding capacitance, there are mature models for normal windings [2, 60, 61], interleaved windings [62], and six-capacitance network considering the intra-winding and inter-winding capacitance of the primary and secondary [8, 63–68]. Most analytical models are based

on the parallel-plate and cylindrical capacitance models and are for the normal winding type I & II [2, 54, 69–71]. For the orthocyclic winding, one solution is to use the parallel-plate and cylindrical capacitance models by modifying the concept of the effective distance between layers [72]. However large errors up to 60% are reported [1]. In [73], the probabilistic distribution of the stray capacitance in various positions is obtained through a generic method. Finally, the models in [74–76] are specially for the orthocyclic winding type IV when the air gap $d_{\rm air} = 0$ in Fig. 1(d). However in reality, due to the hardness of copper wire, there is always irregular curvature in each turn, making $d_{\rm air} > 0$. It causes the overestimation of equations and therefore a modification is necessary.

Until now, there is no systematic study on how the orthocyclic affects all the winding parasitics, i.e., the ac resistance, leakage inductance, and stray capacitance. Our previous research [77] compares the impact through the simulation and experimental results of a series of prototypes. This paper investigates the differences theoretically, and proposes coefficients to modify the equations for orthocyclic windings. It aims to address five aspects:

1) A orthocyclic coefficient is proposed to modify the ac resistance and leakage inductance formula. It compensates magnetic field distortion due to the orthocyclic structure.

2) The new definition of inter-layer insulation distance $a_{\rm iso}$ is proposed for the leakage inductance formula. With that, the energy stored in the inter-layer is considered.

3) For the stray capacitance formula, the equivalent permittivity and equivalent wire diameter are proposed to compensate for the air gap effect.

4) The proposed parasitic equations are verified by finite element method (FEM) simulation and experimental results in four case studies with eight prototypes.

5) Finally, a comprehensive comparison of the orthocyclic and normal winding is given to illustrate its impact to winding parasitics.

The rest of the paper is organized as follows. Section II, III, and IV give the discussion about the impact of the orthocyclic winding to the ac resistance, leakage inductance, and stray capacitance, and proposes coefficients to modify analytical equations. The simulation and experimental comparisons are conducted for verification. Finally, Section V gives a comparison of the difference between orthocyclic and normal windings, and Section VI concludes the paper.

II. AC Resistance of Orthocyclic Winding

A. Dowell's Equation for Ac Resistance

Dowell's equation is originally derived for the normal winding [10]

$$R_{\rm ac} = R_{\rm dc} F_{\rm r} = \frac{l_{\rm MLT} N}{\sigma A} \cdot F_{\rm r} \tag{1}$$

with

$$\begin{aligned} &F_{\rm r} = \triangle[\varsigma + \frac{2}{3}(p^2-1)\xi], \\ &\varsigma = \frac{\sinh(2\triangle)+\sin(2\triangle)}{\cosh(2\triangle)-\cos(2\triangle)}, \qquad \xi = \frac{\sinh\triangle - \sin\triangle}{\cosh\triangle + \cos\triangle}, \\ &\triangle = \frac{\sqrt{\eta} d_{\rm w}}{\delta}, \qquad \eta = \frac{t d_{\rm w}}{h_{\rm c,eq}}, \qquad d_{\rm w} = \frac{\sqrt{\pi}}{2} d_{\rm i} \end{aligned} \tag{2}$$

TABLE I
ORTHOCYCLIC COEFFICIENT $k_{\rm h}$ AT EXTREME CONDITIONS

Winding type	I & II & III	IV
$k_{\rm h}({\rm LF}, \eta_{\rm o})$	1	1
$k_{\rm h}({\rm HF}, 0.5)$	≈ 1	$2/\pi$
$k_{\rm h}({\rm HF}, 1)$	≈ 1	$3/\pi$
$k_{\rm h}({\rm HF}, \eta_{\rm o})$	≈ 1	$\frac{1}{2\eta_{\rm o} \arcsin\frac{1}{2\eta_{\rm o}}}$

[1] Notes: LF : low freq., $\Delta \ll 2$; HF : high freq., $\Delta \gg 6$.

The detailed formulas and parameter definition are in Fig. 2.

B. Orthocyclic Coefficient

Dowell's equations only considers the normal winding type I and II. It assumes the magnetic field flux line is one dimensional, straight, and parallel to the winding, as illustrated by Fig. 2 (b) as the winding type II. In low frequency (LF) range, the skin effect is not distinct and the skin depth δ is much larger than the wire diameter $d_{\rm w}$. So $\Delta \ll 2$, and the flux line is straight. When the frequency increases and $\Delta \gg 6$, there is severe eddy current induced in the wire. They also generate the magnetic fields against the external field. In general, the external fields are pushed out of the wire, and concentrates in the insulation and air gap area between layers. The field itself also slightly distorts as illustrated in the winding type II high frequency (HF) scenario. Nevertheless, Dowell's assumptions are still applicable and these distortions are negligible.

The field intensity H which generates the eddy current loss is

$$H = k_{\rm h}(\Delta, \eta_{\rm o}) \cdot \frac{\rm MMF}{h_{\rm c}} \tag{3}$$

where MMF is the magnetomotive force, Δ is the penetration ratio and has positive correlation with the frequency f, $h_{\rm c}$ is the window height and also the field path length, $k_{\rm h}(\Delta, \eta_{\rm o}) \leq 1$ is the orthocyclic coefficient modifying the field length. $\eta_{\rm o}$ is the new defined orthocyclic porosity factor which uses the winding height $h_{\rm w}$ as denominator

$$\eta_{\rm o} = \frac{t d_{\rm w}}{h_{\rm w}} \tag{4}$$

For the normal winding type I and II, $k_{\rm h}(\Delta, \eta_{\rm o}) = 1$ in low frequency (LF) range, and $k_{\rm h}(\Delta, \eta_{\rm o}) \approx 1$ in high frequency (HF) range. For the orthocyclic winding III with insulator between layers, the wires in each layer is separated by the insulator and keeps a distance from different layers. The effect of the field distortion is weaker than that of the compact orthocyclic type IV. Therefore $k_{\rm h}(\Delta, \eta_{\rm o})$ is close to 1 in HF range, as summarized in Table I.

For compact orthocyclic winding type IV, Dowell's equation overestimates $R_{\rm ac}$ due to the field distortion, as illustrated in Fig. 2 (b). In the low frequency (LF) range, the magnetic field is straight and one-dimensional, $k_{\rm h}(\Delta, \eta_{\rm o}) = 1$. In the high frequency (HF) range, the eddy current induced in the conductor and push the field out of it. Due to the displacement

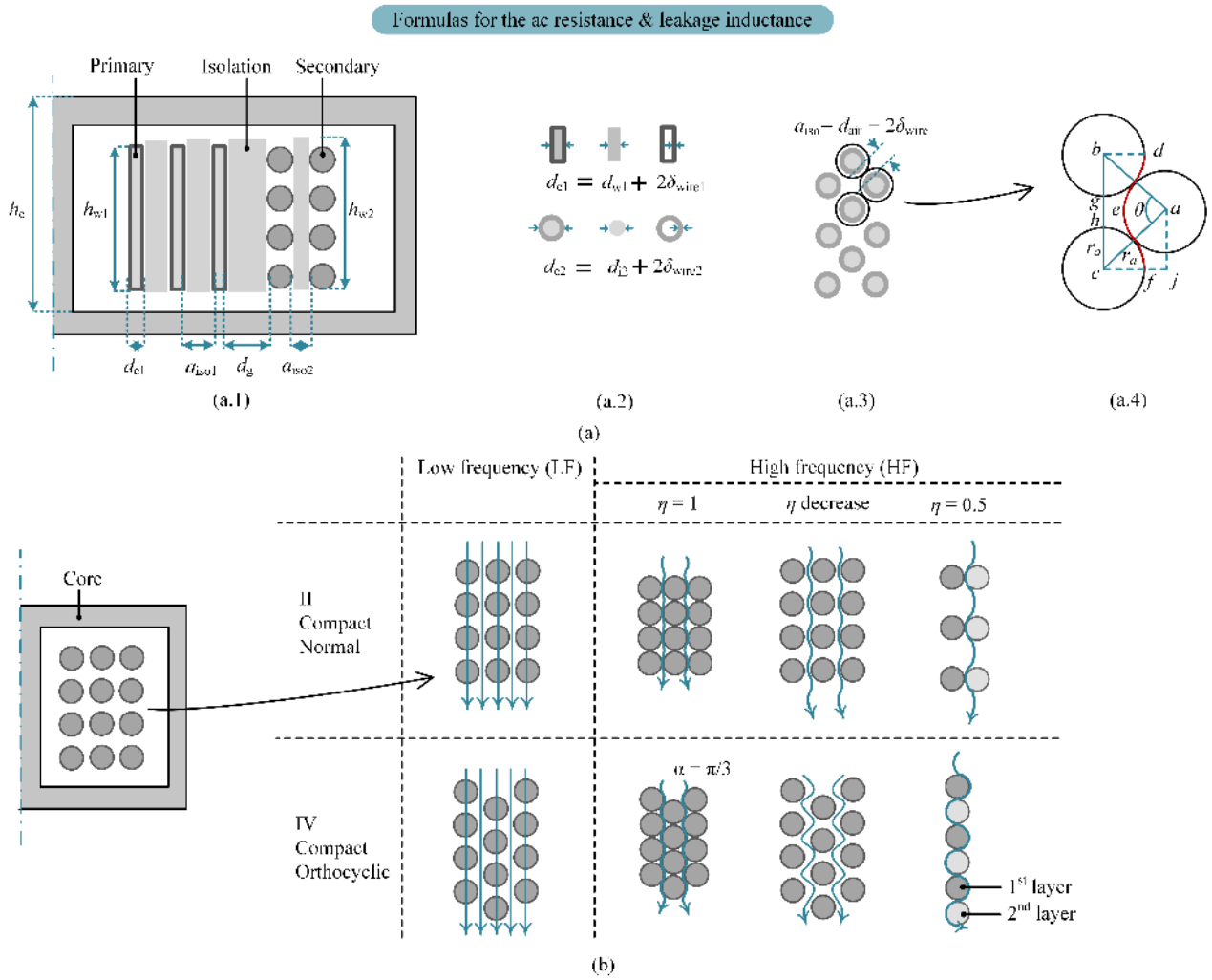

Ac resistance, eq. (1):

$$R_{ac} = R_{dc} F_r$$

where, dc resistance, eq.(1):

$$R_{dc} = \frac{l_{MLT} N}{\sigma A}$$

ac resistance factor, eq. (8):

$$F_r = \Delta[\varsigma - k_h(\Delta, \eta_o)^2 \cdot \frac{2}{3}(p^2 - 1)\xi]$$

skin coefficient ς & proximity effect ξ, eq. (2):

$$\varsigma = \frac{\sinh(2\Delta) - \sin(2\Delta)}{\cosh(2\Delta) - \cos(2\Delta)}, \qquad \xi = \frac{\sinh\Delta - \sin\Delta}{\cosh\Delta + \cos\Delta}$$

Penetration ratio Δ, eq. (2):

$$\Delta = \frac{\sqrt{\eta} d_w}{2\delta} \qquad d_w = \frac{\sqrt{\pi}}{2} d_i$$

where, porosity factor η and orthocyclic porosity factor η_o, eq.(2. 4):

$$\eta = \frac{t d_w}{h_{w,eq}} \qquad \eta_o = \frac{t d_w}{h_w}$$

Equivalent field length $h_{c,eq}$ and winding length $h_{w,eq}$, orthocyclic coefficient k_h eq.(7, 9, 12):

- Winding type I, II, III

$$h_{c,eq} = h_c \qquad h_{w,eq} = h_w \qquad k_h(\Delta, \eta_o) = 1$$

- Winding type IV

$$h_{c,eq} = h_c / k_h(\Delta, \eta_o) \qquad h_{w,eq} = h_w / k_h(\Delta, \eta_o)$$

$$k_h(\Delta, \eta_o) = \frac{\frac{1}{\sin\frac{\pi}{3}\sqrt{\frac{\pi}{4\eta_o}}}}{2} \left[1 + \tanh\left(\frac{\Delta}{2} - 4\right)\right] + \frac{\frac{1}{\sqrt{\eta_o}\sin\frac{\pi}{3}\sqrt{\frac{\pi}{4\eta_o}}}}{2}\left[1 - \tanh\left(\frac{\Delta}{2} - 4\right)\right]$$

Ac leakage inductance, eq. (10):

$$L_\sigma = \mu_0 N_1^2 \frac{l_{MLT}}{h_{w,eq}} \left[d_{w1} \frac{p_1}{3} F_{L1} + d_{w2} \frac{p_2}{3} F_{L2} + d_g + a_{iso1} \frac{(p_1 - 1)(2p_1 - 1)}{6p_1} + a_{iso2} \frac{(p_2 - 1)(2p_2 - 1)}{6p_2} \right]$$

where, leakage inductance factor, eq. (11):

$$F_{L1} = \frac{1}{2p_1^2 \Delta_1} [(4p_1^2 - 1)\varphi_a - 2(p_1^2 - 1)\varphi_b]$$

$$\varphi_a = \frac{\sinh(2\Delta_1) - \sin(2\Delta_1)}{\cosh(2\Delta_1) - \cos(2\Delta_1)}, \qquad \varphi_b = \frac{\sinh\Delta_1 - \sin\Delta_1}{\cosh\Delta_1 - \cos\Delta_1}$$

- l_{MLT} : the mean length per turn of the winding
- N : the number of turns of the winding
- σ : the conductivity of the wire
- A : the cross section area of each turn
- Δ : the penetration ratio of the wire
- η : the porosity factor
- η_o : the orthocyclic porosity factor
- p : the number of layers of the winding
- d_i : the bare diameter of the round wire without coating
- d_w : the width of the foil without coating
- δ : the skin depth of the frequency of interest
- μ_0 : the permeability of air
- t : the number of turns per layer
- h_c : the height of the core window
- h_w : the height of the winding
- d_g : the thickness of the inter-winding insulation
- a_{iso} : the inter-layer insulation distance in width direction, including wire coating, airgap, and layer insulation
- F_{L2} : the inductance factor of secondary, similar to F_{L1} except for that p_1 and Δ_1 replaced by p_2 and Δ_2

(c)

Fig. 2. Formulas for the winding resistance and inductance. (a.1) Cross-section the transformer. (a.2) Wire dimensions. (a.3) Definition of the a_{iso} in orthocyclic winding type IV for the leakage inductance calculation. (a.4) Dimension definition to calculate the distorted field length analytically. (b) The field distortion of winding type II and IV with respect to the frequency. Winding type I and III are similar to II and are neglected. (c) The ac resistance and leakage inductance formulas.

of the wire position, the field distortion of compact orthocyclic winding is much severe than normal winding. A geometrical relation between the wire diameter and the field length is illustrated in Fig. 2 (a.4).

Define the angle of $\angle\ bac$ as θ, and r_a is the sum of the wire radius δ_wire and half of the air gap length $d_\mathrm{air}/2$. In Fig. 2 (a.4), the orthocyclic porosity factor η_o is expressed as $\eta_\mathrm{o} = 2r_\mathrm{a}/(2r_\mathrm{a} + l_{gh})$, where l_{gh} is the length of the line gh. Moreover, there are relation between the angle θ and l_{gh}: $4r_\mathrm{a}\sin(\theta/2) = 2r_\mathrm{a} + l_{gh}$. Substituting l_{gh} of two equations obtains the relationship between the orthocyclic porosity factor η_o and the angle θ

$$\theta = 2\arcsin\frac{1}{2\eta_\mathrm{o}} \tag{5}$$

The length of line bc is $2\times 2r_\mathrm{a}\sin(\theta/2) = 4r\sin(\theta/2)$. The red curve def is approximately the length of the orthocyclic magnetic field flux, its length is $2r_\mathrm{a}\theta$. So the flux of orthocyclic winding is $1/k_\mathrm{h}(\Delta,\eta_\mathrm{o})$ times longer than normal winding in high frequency (HF) range

$$k_\mathrm{h}(\mathrm{HF},\eta_\mathrm{o}) = \frac{4r_\mathrm{a}\sin(\theta/2)}{2r_\mathrm{a}\theta} = \frac{1}{2\eta_\mathrm{o}\arcsin\frac{1}{2\eta_\mathrm{o}}} \tag{6}$$

According to (6), $k_\mathrm{h}(\mathrm{HF},\eta_\mathrm{o}) = 3/\pi$ when $\eta_\mathrm{o} = 1$, $k_\mathrm{h}(\mathrm{HF},\eta_\mathrm{o}) = 2/\pi$ when $\eta_\mathrm{o} = 0.5$. When $0.5 \le \eta_\mathrm{o} \le 1$, $3/\pi \le k_\mathrm{h}(\mathrm{HF},\eta_\mathrm{o}) \le \pi/2$.

Table I summarizes the quantitative relation between $k_\mathrm{h}(\Delta,\eta_\mathrm{o})$ and η_o. For the relationship between $k_\mathrm{h}(\Delta,\eta_\mathrm{o})$ and penetration ratio Δ (Δ is positive correlation to frequency f), a qualitative conclusion is reached: in low frequency (LF) range ($\Delta \le 2$), $k_\mathrm{h}(\Delta,\eta_\mathrm{o}) = 1$; in high frequency (HF) range ($\Delta \ge 6$), $k_\mathrm{h}(\Delta,\eta_\mathrm{o}) = \frac{1}{2\eta_\mathrm{o}\arcsin\frac{1}{2\eta_\mathrm{o}}}$. To quantify this relation, a Hyperbolic function $\tanh$ is used

$$\begin{aligned} &k_\mathrm{h}(\Delta,\eta_\mathrm{o}) \\ &= \frac{k_\mathrm{h}(\mathrm{HF},\eta_\mathrm{o})-1}{2}\tanh(\frac{\Delta-4}{2}) + \frac{k_\mathrm{h}(\mathrm{HF},\eta_\mathrm{o})+1}{2} \\ &= \frac{\frac{1}{2\eta_\mathrm{o}\arcsin\frac{1}{2\eta_\mathrm{o}}}-1}{2}\tanh(\frac{\Delta-4}{2}) + \frac{\frac{1}{2\eta_\mathrm{o}\arcsin\frac{1}{2\eta_\mathrm{o}}}+1}{2} \end{aligned} \tag{7}$$

when $\Delta \le 2$, then $\frac{\Delta-4}{2} \le -1$ and $\tanh(\frac{\Delta-4}{2}) \approx -1$, so $k_\mathrm{h}(\Delta,\eta_\mathrm{o}) \approx 1$; when $\Delta \ge 6$, then $\frac{\Delta-4}{2} \ge 1$ and $\tanh(\frac{\Delta-4}{2}) \approx 1$, so $k_\mathrm{h}(\Delta,\eta_\mathrm{o}) \approx k_\mathrm{h}(\mathrm{HF},\eta_\mathrm{o})$; when $2 \le \Delta \le 4$, $k_\mathrm{h}(\Delta,\eta_\mathrm{o})$ locates in between. $\tanh$ function acts as a switch to give the value between the extreme values in Table I. So the orthocyclic coefficient (7) gives the relation between $k_\mathrm{h}(\Delta,\eta_\mathrm{o})$, Δ, and η_o. (7) can also be other form of functions.

Compared with the assumptions of Dowell's equation for normal winding, the field length of the orthocyclic winding is $1/k_\mathrm{h}(\Delta,\eta_\mathrm{o})$ times longer, and the field intensity is $k_\mathrm{h}(\Delta,\eta_\mathrm{o})$ times smaller. Therefore, $k_\mathrm{h}(\Delta,\eta_\mathrm{o})$ is used to compensate Dowell's equation for the orthocyclic winding effect, referring to [16] using η to compensate the magnetic field for the porosity effect. So the ac resistance factor F_r and equivalent window height is modified to

$$F_\mathrm{r} = \triangle[\varsigma + k_\mathrm{h}(\Delta,\eta_\mathrm{o})^2\cdot\frac{2}{3}(p^2-1)\xi], \tag{8}$$

$$h_\mathrm{c,eq} = h_\mathrm{c}/k_\mathrm{h}(\Delta,\eta_\mathrm{o}) \tag{9}$$

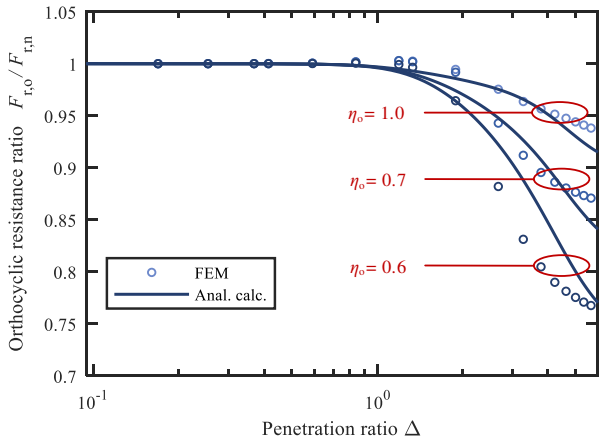

Fig. 3. Orthocyclic resistance ratio $F_{\mathrm{r,o}}/F_{\mathrm{r,n}}$ with respective to the penetration ratio Δ and orthocyclic porosity factor η_o. The circle is the simulation results. The solid line is the analytical calculated results.

TABLE II
TRANSFORMERS WITH NORMAL AND ORTHOCYCLIC WINDINGS

Parameters	P1/ P1o	P2/ P2o	P3/ P3o	Units
ETD Core	59/31/22	59/31/22	29/16/10	
Pri./Sec. p	3	3	3	
Layer turns t	34	30	20	
Wire Dia. d_i	1.0	0.9	0.75	mm
Main Insu. d_g	0.8	0.4	0.2	mm
Inter-layer a_iso	0.2	0.1	0.1	mm

Substituting (8) and (9) into (1) and (2) obtains modified equation for the orthocyclic winding.

To verify the proposed orthocyclic coefficient, two groups of transformers with the same ETD 59/31/22 core, 3 layers primary and secondary winding, 1 mm wire diameter, 0.8 mm main insulation, 0.2 mm inter-layer insulation, but different winding configurations are designed and simulated. The first group is with normal winding, and the second is with orthocyclic winding. In each group, there are three transformers with the number of turns per layer t as 40, 27, 23, which results in the orthocyclic porosity factor η_o as 1.0, 0.7, and 0.6, respectively. Defining Dowell's ac resistance factor for normal winding as $F_{\mathrm{r,n}}$, the modified ac resistance factor for orthocyclic winding as $F_{\mathrm{r,o}}$, their ratio $F_{\mathrm{r,o}}/F_{\mathrm{r,n}}$ in Fig. 3 shows a good agreement between the simulation and calculation.

The orthocyclic factor is different from the porosity factor. The porosity factor modifies the magnetic field prolongation due to the air gap between turns with η. The orthocyclic factor considers the prolongation due to the orthocyclic placement. They can be used at the same time to modify the field distortion.

C. FEM and Experimental Verification: Three Case Studies

1) Case 1: ETD 59/31/22 core, $\eta_\mathrm{o} = 0.91$: To verify the proposed equation for winding IV, two transformers are

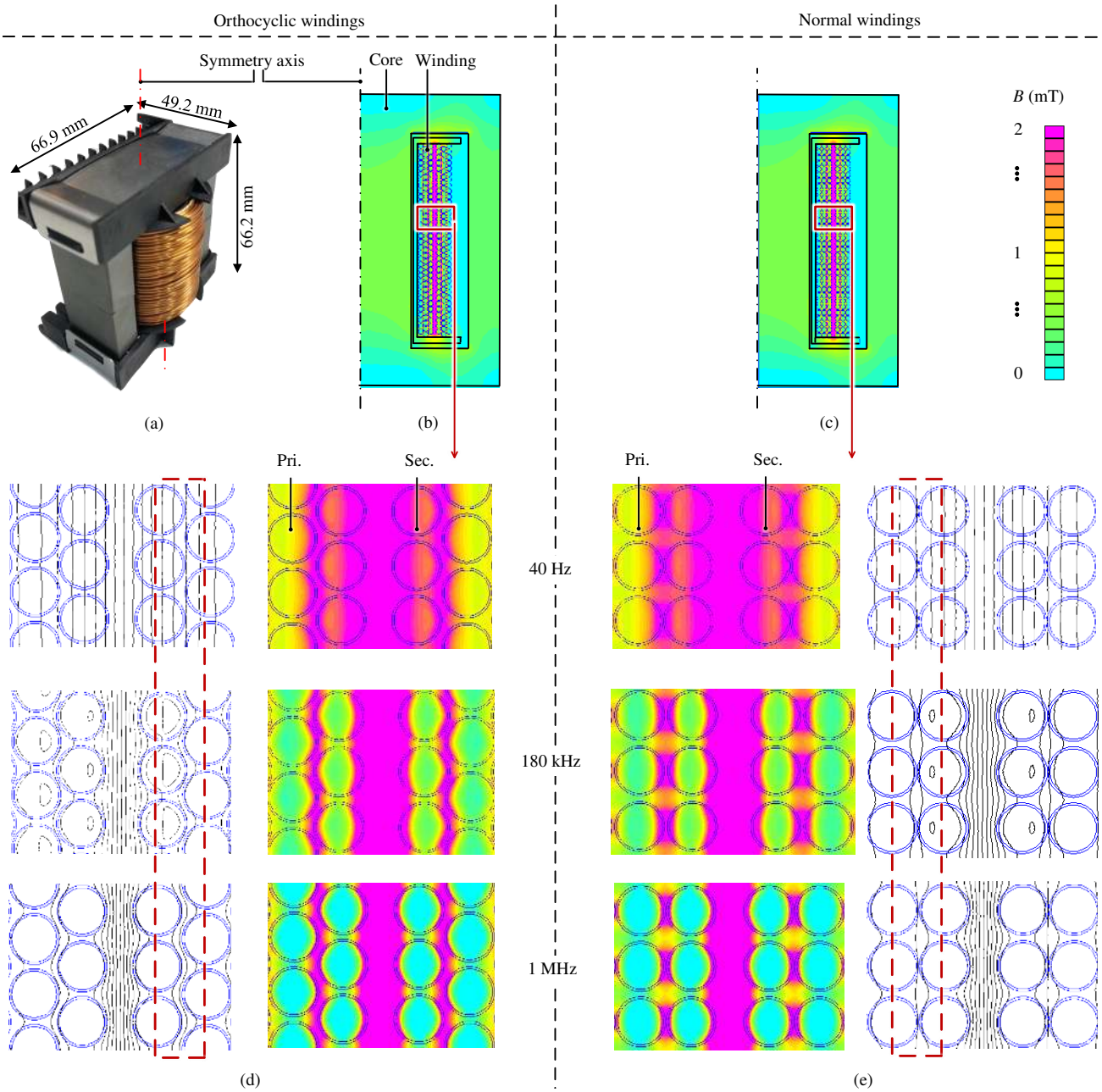

Fig. 4. The prototype and magnetic field simulation of P1 and P1o. (a, b, d) Prototype and simulation of P1o with winding type IV, and its zoom-in view. (c, e) Simulation of P1 with winding type II and its zoom-in view. The magnetic field in (d) and (e) verifies the field distortion illustration in Fig. 2(b). The magnetic flux density are plotted here while the filed strength in the window area follows the similar distribution with a coefficient of the permeability μ_0.

designed named P1 and P1o as in Table II, respectively. P1 is with the winding type II and P1o is IV. They are with the same winding distance d_g, inter-layer distance $a_{\rm iso}$, core, and bobbin. Only P1o is built because wiring the winding II is difficult. The finite element method (FEM) simulation results in Fig. 4 show the magnetic field of two windings from low to high frequency, which verifies the field illustration in Fig. 2(b).

The experimental comparison is in Fig. 5 (a, b). In practice, the porosity factors are calculated directly using (4), the vertical distance of wires at adjacent layers $l_{\rm aj}$ in Fig. 2(a.4) is calculated by

$$l_{\rm aj} = \frac{h_{\rm w} - d_{\rm e}}{2(t-1)} \tag{10}$$

the horizontal distance of wires at adjacent layers $l_{\rm cj}$ is

$$l_{\rm cj} = \frac{d_{\rm wdg} - d_{\rm e}}{p-1} \tag{11}$$

where $d_{\rm wdg}$ is the width of the winding, the air-gap between the wires $d_{\rm air}$ is

$$d_{\rm air} = \sqrt{l_{\rm aj}^2 + l_{\rm cj}^2} - d_{\rm e} \tag{12}$$

and the vertical distance between each equivalent turn $l_{\rm gh}$ is

$$l_{\rm gh} = 2l_{\rm aj} - d_{\rm e} - d_{\rm air}. \tag{13}$$

The simulation is close to the measurement results. For the analytical results, if the original Dowell's equation for the normal winding is used for the orthocyclic winding, it overestimates the ac resistance in most of the frequency points, and the maximum error is 9.8%. If the modified equation with orthocyclic coefficient is used, the maximum error reduces to 4.7%.

Wiring the exact winding II and IV are difficult in reality. Due to the clock and counterclockwise of the spiral in neighborhood layers, the wires stay in a position which is between type II and IV, but more turns are close to type IV. Therefore the measurement value, the normal equation, and the orthocyclic equation are all with errors compared with the measurements. Moreover, the orthocyclic equation is with smaller error than normal equations.

2) Case 2: ETD 59/31/22 core, $\eta_{\rm o} = 0.73$: Two transformers P2 with winding II and P2o with IV are designed as in Table II, respectively. The experimental comparison is in Fig. 5 (c, d). It shows that this field distortion is more severe with the decrease of the orthocyclic porosity factor $\eta_{\rm o}$, and the orthocyclic equation offers smaller error (max 8.4%) than Dowell's equation (max 20.3%).

3) Case 3: ETD 29/16/10 core, $\eta_{\rm o} = 0.87$: Transformers P3 and P3o are also with winding II and IV but smaller cores, as in Table II. The test results are in Fig. 5 (e, f). The maximum error of Dowell's equation is 16.2%, while it is 9.4% for orthocyclic equation.

Compared with Dowell's equation for the normal winding, the orthocyclic equation compensates the field distortion and achieves better accuracy in most frequency range, while at the remaining frequency, e.g., 20 and 40 kHz, their difference are negligible.

In general, the accuracy of the proposed equation is improved for the orthocyclic windings, especially with the decrease of the orthocyclic porosity factor and increase of the frequency. The maximum error of the proposed equation in three cases is 8.6%, while Dowell's equation 24.4%. On the other side, the error of orthocyclic equation still follows the error of Dowell's equation with the increase of frequency, because it is a modify coefficient based on Dowell's equation, and they share the similar field assumptions.

III. Leakage Inductance of Orthocyclic Winding

A. Analytical Model for Leakage Inductance

The ac leakage inductance represents the energy storage ability of the winding. It consists of the frequency-dependent and independent parts [10, 47, 78]

$$L_\sigma = \mu_0 N_1^2 \frac{l_{\rm LMT}}{h_{\rm w,eq}} [\underbrace{d_{\rm w1}\frac{p_1}{3}F_{L1} + d_{\rm w2}\frac{p_2}{3}F_{L2}}_{\text{freuqncy dependent}} + \underbrace{d_{\rm g} + a_{\rm iso1}\frac{(p_1-1)(2p_1-1)}{6p_1} + a_{\rm iso2}\frac{(p_2-1)(2p_2-1)}{6p_2}}_{\text{freuqncy independent}}] \tag{14}$$

where

$$F_{L1} = \frac{1}{2p_1^2\triangle_1}[(4p_1^2-1)\varphi_{\rm a} - 2(p_1^2-1)\varphi_{\rm b}],$$
$$\varphi_{\rm a} = \frac{\sinh(2\triangle_1)-\sin(2\triangle_1)}{\cosh(2\triangle_1)-\cos(2\triangle_1)}, \quad \varphi_{\rm b} = \frac{\sinh\triangle_1 - \sin\triangle_1}{\cosh\triangle_1 - \cos\triangle_1} \tag{15}$$

F_{L1} is the leakage inductance factor of primary winding. The formula and parameter definitions are also in Fig. 2.

B. Orthocyclic Coefficient & Inter-layer Distance

For orthocyclic winding IV, the magnetic field length increases and the field intensity H also decreases to (3). The weaken of the field intensity also decreases the leakage inductance. The winding height $h_{\rm w}$ in (14) is modified by the orthocyclic factor

$$h_{\rm w,eq} = h_{\rm w}/k_{\rm h}(\Delta, \eta_{\rm o}) \tag{16}$$

Besides, the original definition of the inter-layer insulation distance $a_{\rm iso}$ is in the horizontal direction, as in Fig. 1 and Fig. 2 (a.1). It is close to zero or even negative for orthocyclic winding IV . So the leakage flux in the inter-layer is neglected, which leads to the underestimation of the formula. The newly defined $a_{\rm iso}$ is the direct distance between two wires in adjacent layers, as in Fig. 2 (a.3). It depicts the width of the magnetic field path in reality.

Substituting (16) and the new defined inter-layer insulation distance $a_{\rm iso}$ into (14) obtains the proposed leakage inductance for orthocyclic windings, as summarized in Fig. 2.

C. Finite Element Method and Experimental Verification

Transformers P1o, P2o, and P3o in the previous section are also used to verify the proposed leakage inductance formula with the the orthocyclic factor and newly defined inter-layer $a_{\rm iso}$, as in Fig.6.

There is error of the simulation results compared with the measurement. This is due to that the winding position in reality is between type II and IV, as indicated in the previous section. With the decrease of frequency, the eddy current effect in both winding and core decreases and the measured short-circuit inductance increases [11]. When close to zero frequency, the impedance of the main inductance falls to the comparable value with the resistive component and it cannot be neglected when short-circuited. Therefore the measurement is not accurate anymore, and the error at 0 Hz is significant.

For analytical calculation, Anal. Norm is the original equation (14) for the orthocyclic winding, Anal. Norm + $k_{\rm h}$ comp. is the original equation (14) plus the modified winding height (16) for the orthocyclic winding, and Anal. Orc is the proposed equation for the orthocyclic winding.

In all three cases, the Anal. Norm and Anal. Norm + $k_{\rm h}$ comp. are with similar accuracy. So the impact of the field distortion to the leakage inductance is not significant. However, with the change of the definition of $a_{\rm iso}$, the proposed orthocyclic equation achieves much smaller error compared with those two equations. It indicates that neglecting or the unsuitable definition of the inter-layer insulation distance $a_{\rm iso}$ causes the significant underestimation.

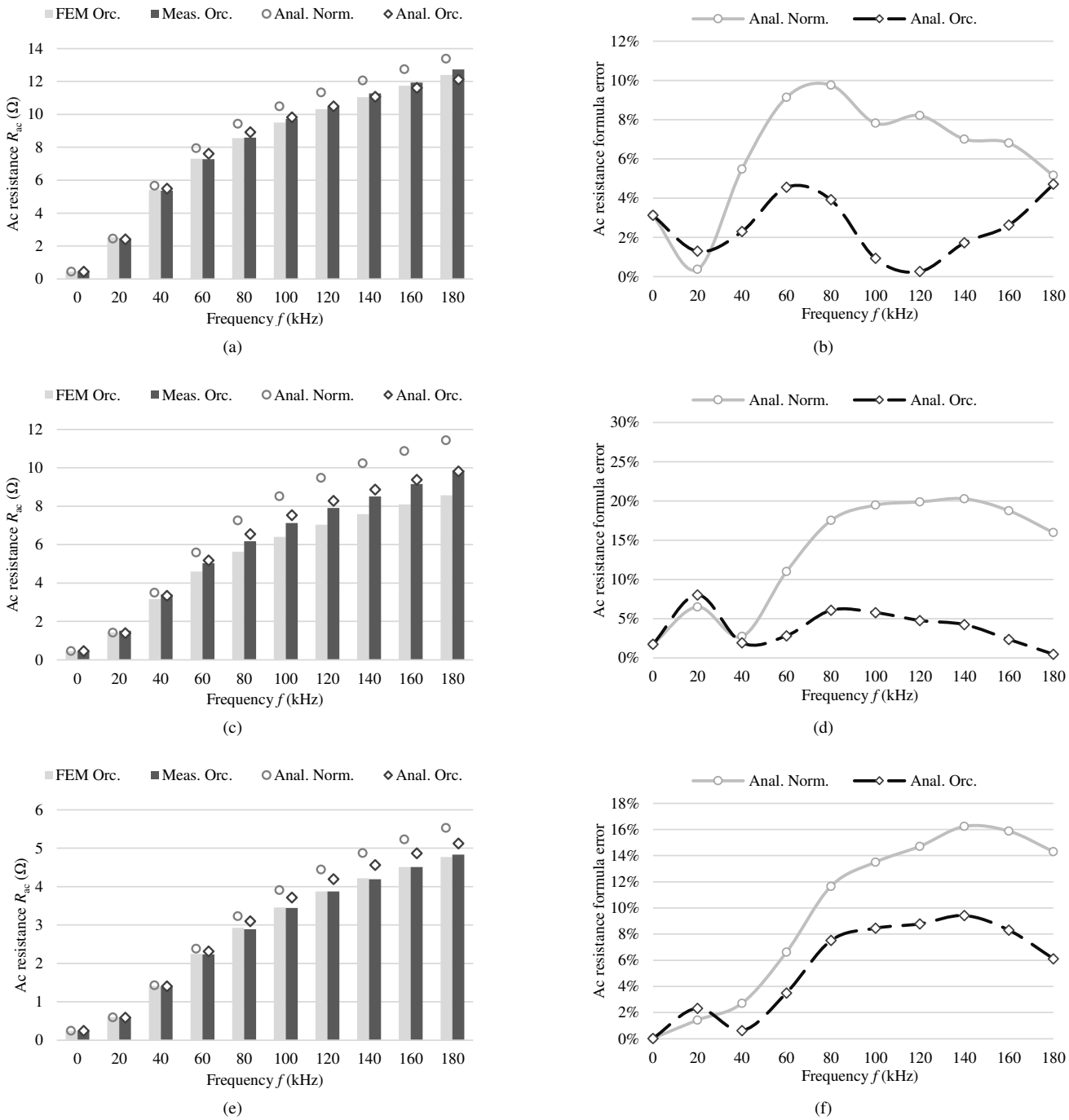

Fig. 5. Ac resistance of transformers with orthocyclic windings. FEM Orc., Anal. Orc., and Meas. Orc. are the FEM, analytical, and measurement results of the prototype with orthocyclic winding type IV, respectively. Dowell's equation for the normal winding is also used to calculate the orthocyclic winding, as marked with Anal. Norm. (a) Ac resistance of the Prototype P1o. (b) Error of the analytical equation compared with the experimental results. (c), (d), (e), and (f) are the ac resistance and analytical formula error of prototypes P2o and P3o, respectively.

Finally, the change of errors of the proposed equation follows with the original, which is due to the similar Dowell's field assumption.

IV. Stray Capacitance of Orthocyclic Winding

A. Parallel-Plate Model for Normal Winding

The classic parallel-plate model for layer capacitance C_{ww} is

$$C_{\mathrm{ww,n}} = \varepsilon_0 \varepsilon_{\mathrm{wire}} \frac{2\pi h_{\mathrm{w}} (l_{\mathrm{MLT}}/(2\pi))}{d_{\mathrm{ww}}} \tag{17}$$

The winding total capacitance C_{w} is obtained by connecting

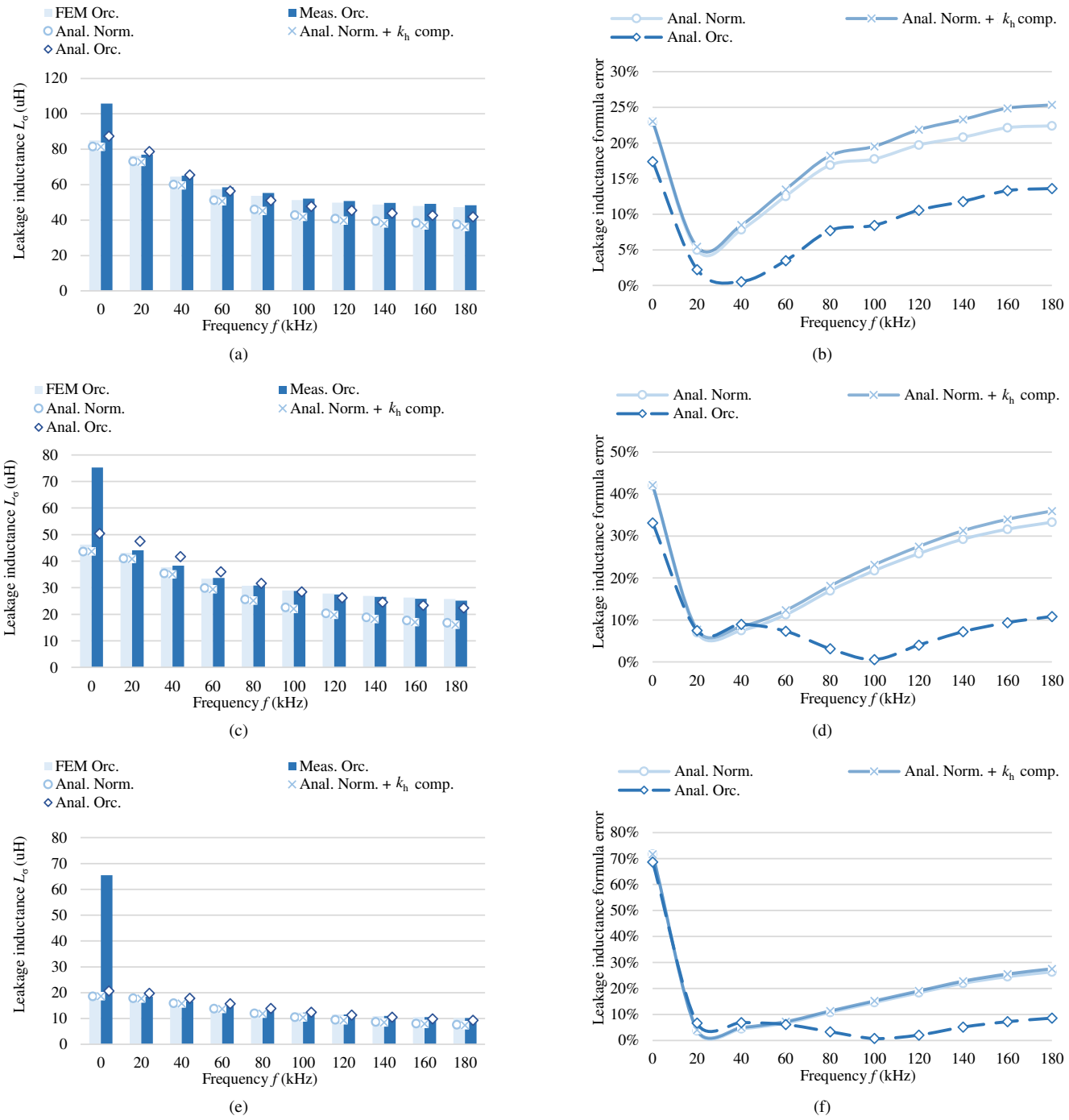

Fig. 6. Leakage inductance of transformers with orthocyclic windings. FEM Orc., Anal. Orc., and Meas. Orc. are the FEM, analytical, and measurement results of the prototype with orthocyclic winding type IV, respectively. Dowell's equation for the normal winding and Dowell's equation plus the orthocyclic coefficient k_h compensation are also used to calculate the orthocyclic winding, as marked with Anal. Norm. and Anal. Norm. + k_h comp. (a) Leakage inductance of the Prototype P1o. (b) Error of the analytical equation compared with the experimental results. (c), (d), (e), and (f) are the leakage inductance and analytical formula error of prototypes P2o and P3o, respectively.

the layer capacitance C_l in each layer [79]

$$C_w = \beta \cdot C_{ww}(p-1)(\frac{2}{p})^2 \tag{18}$$

The formulas and the definitions of parameters are in Fig. 7.

B. Basic Cell Model for Orthocyclic Winding

The parallel-plate model has the significant error for orthocyclic windings [1]. An alternative formula in [72, 75] is based on the field analysis in basic cells of winding IV in Fig. 7. It is used in [1] to calculate the layer capacitance of the orthocyclic winding without insulation layer:

$$C_{ww,o} = t\varepsilon_0 \frac{4\varepsilon_{wire} \arctan\left[\frac{(\sqrt{3}-1)(2\varepsilon_{wire}+k_{ln})}{(\sqrt{3}+1)\sqrt{k_{ln}(2\varepsilon_{wire}+k_{ln})}}\right]}{\sqrt{2\varepsilon_{wire}k_{ln}+k_{ln}^2}} \tag{19}$$

where $k_{ln} = \ln k_{rad}$, $k_{rad} = d_e/d_i$ is the radius ratio, d_e and

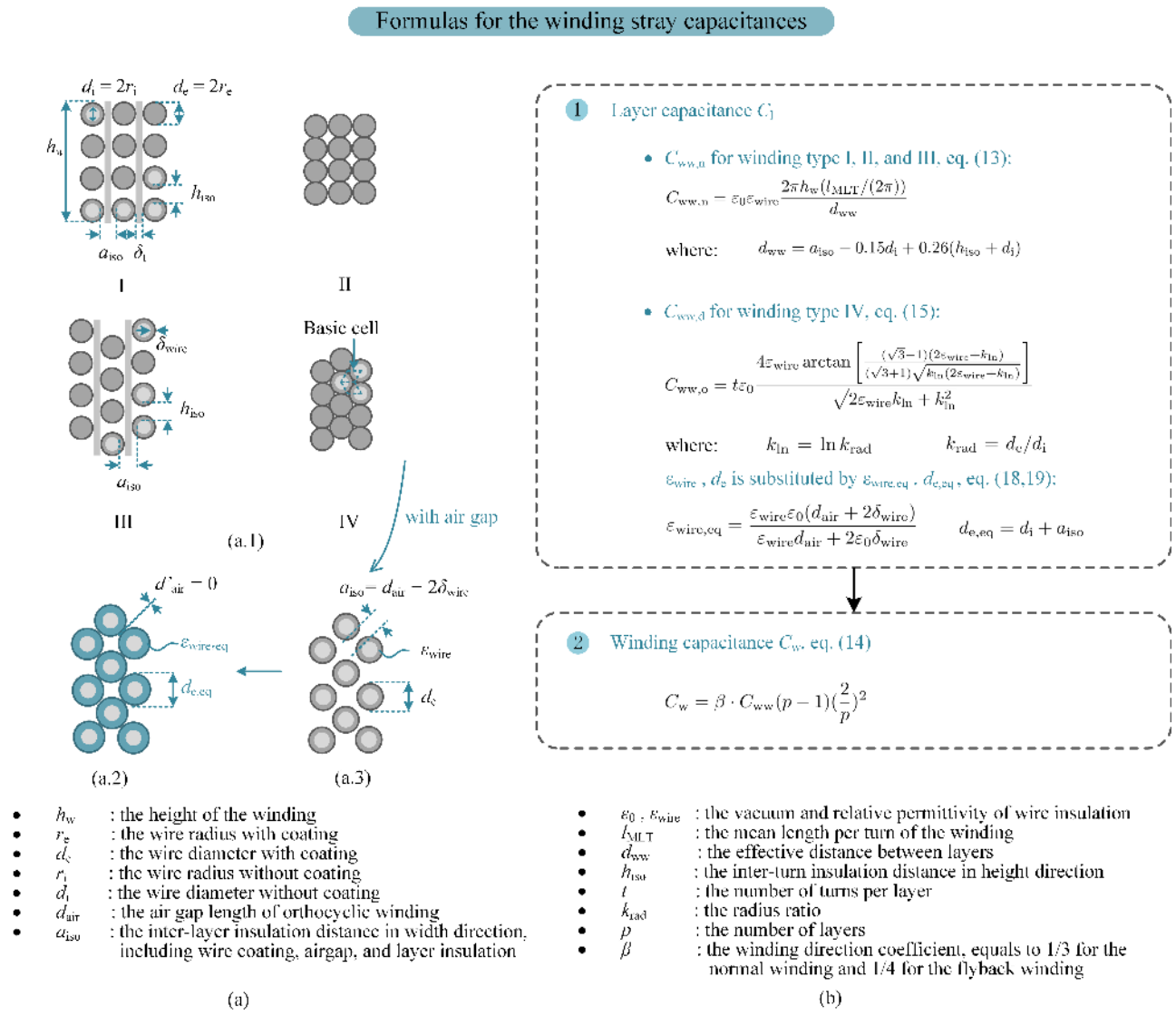

Fig. 7. Stray capacitance formulas of the normal and orthocyclic windings. (a) Wire dimension definition. (a.1) is four typical windings types. (a.2) is the transformation of the winding type IV from with air gaps to without gaps, with the equivalent permittivity $\varepsilon_{wire,eq}$ and equivalent diameter $d_{e,eq}$. (a.3) is the definition of a_{iso} of the winding type IV with air gaps between turns in adjutant layers. (b) Winding capacitance formulas.

TABLE III
INDUCTORS WITH NORMAL AND ORTHOCYCLIC WINDINGS

Parameters	Normal L2,3,4,5,8	Orthocyclic L2o,3o,4o,5o,8o	Units
Core type	ETD 59/31/22		
Layers p	2, 3, 4, 5, 8		
Layer turns t	34		
Wire dia. d_i	1		mm
Wire iso. δ_{wire}	0.05		mm
Inter-layer a_{iso}	0.13		mm

d_i are the diameter of the wire with and without insulation coating, respectively, t is the number of turns per layer. Other parameters are illustrated in Fig. 7.

C. Compensation Equations for Orthocyclic Winding

Equation (19) is derived when the air gap length $d_{air} = 0$ in the basic cell of Fig. 7(a.1) type IV. So it requires no air gap between layers. In reality, wiring the compact winding IV is difficult. Due to the hardness of the copper wire, there is normally air-gap between layers and $d_{air} > 0$, as in Fig. 7 (a.3). So (19) only considers the insulation coating between two bare conductors with the thickness of $2\delta_{wire}$. It overestimates the layer capacitance when there is air between two wires and $d_{air} > 0$.

To compensate the air gap effect, the system 1: *conductor 1-coating 1-air gap-coating 2-conductor 2* is transferred to the system 2: *conductor 1-coating 1-coating 2-conductor 2*, as from Fig. 7(a.3) to (a.2). Through the transferring, the thickness of the wire coating δ_{wire} increases to $\delta_{wire} + d_{air}/2$ and leads to $d'_{air} = 0$, so the assumptions for (19) is valid again.

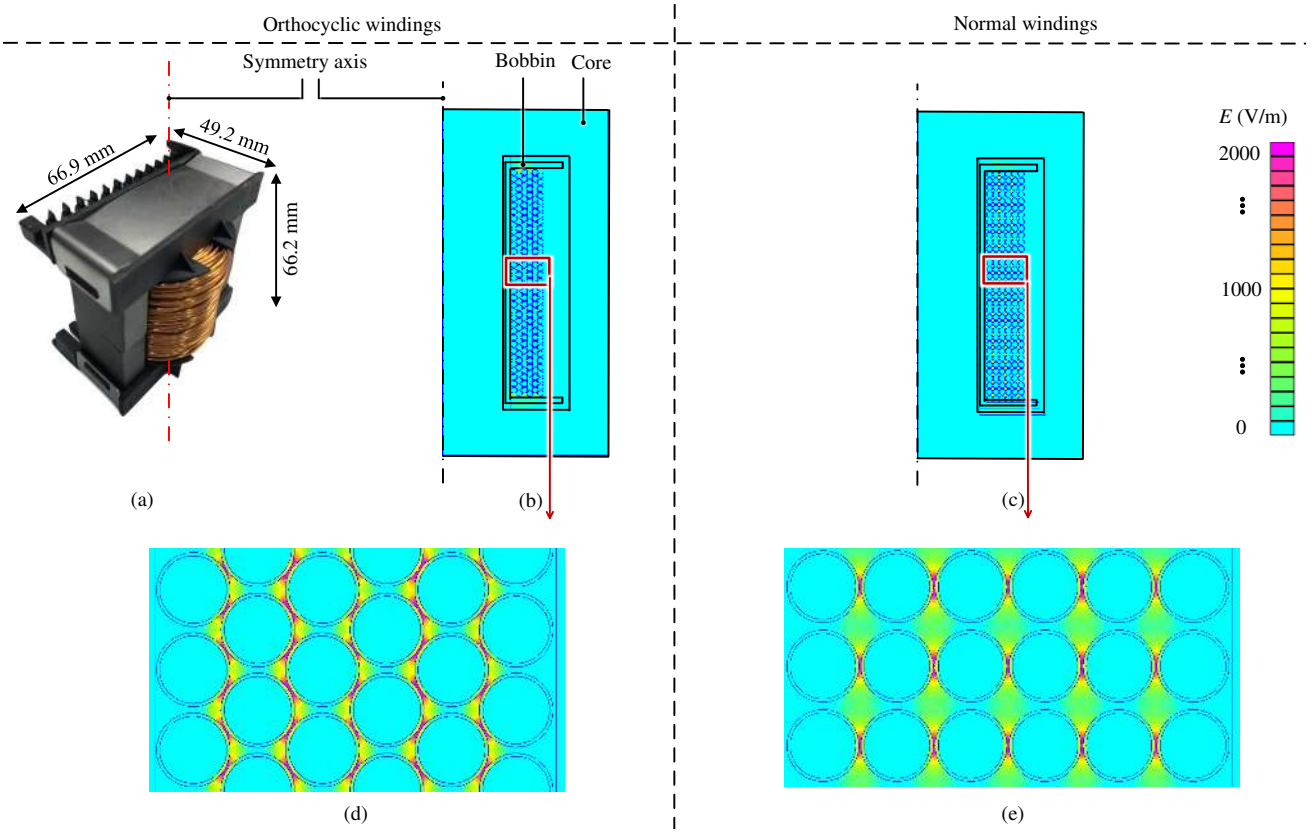

Fig. 8. The prototype and electrical field simulation of Prototype L8 and L8o. (a, b, d) Prototype and simulation of L8o, and its zoom-in view. (c, e) Simulation of L8 and its zoom-in view.

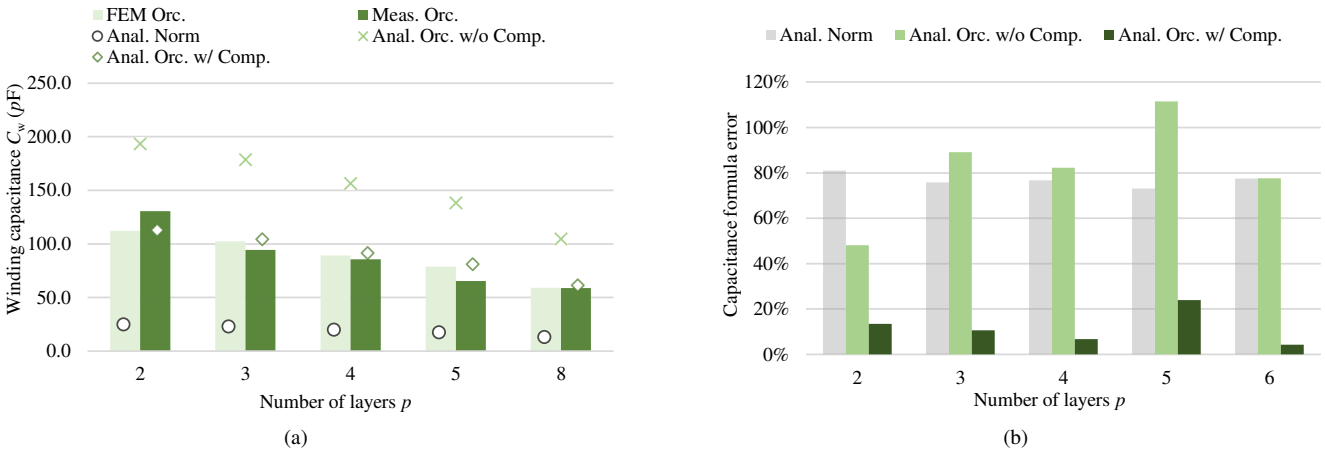

Fig. 9. Stray capacitance of inductors with orthocyclic windings. (a) The FEM, analytical, and measurement result of the inductor L2o, L3o, L4o, L5o, L8o are marked as FEM Orc., Anal. Orc. w/ Comp., and Meas. Orc., respectively. The analytical result with (17) and with (19) but without equivalent permittivity and diameter compensation equations (22, 23) are also presented as Anal. Norm. and Anal. Orc. w/o Comp.. The core-related capacitance is subtracted in all cases [58]. (b) Error of the analytical equations compared with the experimental results.

Referring to the transferring method in [1] for the parallel plate model, the equivalent permittivity and capacitance distance is also modified here for the orthocyclic winding. In system 1, the capacitance between conductor 1 and 2 are the series connection of the coating 1 capacitance C_{co1}, air gap capacitance C_{ag}, and coating 2 capacitance C_{co2}, respectively. $C_{\mathrm{co1}} = C_{\mathrm{co2}}$ due to the same type of wire and coating. Their total capacitance C_{tot} is the series connecting of three capacitances

$$C_{\mathrm{tot}} = \frac{1}{\frac{1}{C_{\mathrm{co1}}} + \frac{1}{C_{\mathrm{ag}}} + \frac{1}{C_{\mathrm{co2}}}} = \frac{C_{\mathrm{co1}} C_{\mathrm{ag}}}{C_{\mathrm{co1}} + 2C_{\mathrm{ag}}} \tag{20}$$

Assume C_{co1} and C_{ag} are with the same capacitance area A_{co}, their permittivity and capacitance distance are $\varepsilon_{\mathrm{wire}}$, ε_0, δ_{wire},

and d_{air}, respectively. So (20) becomes

$$\begin{aligned} C_{\mathrm{tot}} &= \frac{\frac{\varepsilon_{\mathrm{wire}} A_{\mathrm{co}}}{\delta_{\mathrm{wire}}} \frac{\varepsilon_0 A_{\mathrm{co}}}{d_{\mathrm{air}}}}{\frac{\varepsilon_{\mathrm{wire}} A_{\mathrm{co}}}{\delta_{\mathrm{wire}}} + 2\frac{\varepsilon_0 A_{\mathrm{co}}}{d_{\mathrm{air}}}} \\ &= \frac{\varepsilon_{\mathrm{wire}}\varepsilon_0(d_{\mathrm{air}} + 2\delta_{\mathrm{wire}})}{\varepsilon_{\mathrm{wire}} d_{\mathrm{air}} + 2\varepsilon_0\delta_{\mathrm{wire}}} \frac{A_{\mathrm{co}}}{d_{\mathrm{air}} + 2\delta_{\mathrm{wire}}} \\ &= \varepsilon_{\mathrm{wire,eq}} \frac{A_{\mathrm{co}}}{a_{\mathrm{iso}}} \end{aligned} \tag{21}$$

Therefore, from Fig. 7 (a.3) to (a.2), the original $\varepsilon_{\mathrm{wire}}$ is modified to the equivalent permittivity $\varepsilon_{\mathrm{wire,eq}}$

$$\varepsilon_{\mathrm{wire,eq}} = \frac{\varepsilon_{\mathrm{wire}}\varepsilon_0(d_{\mathrm{air}} + 2\delta_{\mathrm{wire}})}{\varepsilon_{\mathrm{wire}} d_{\mathrm{air}} + 2\varepsilon_0\delta_{\mathrm{wire}}} \tag{22}$$

the diameter of the wire with coating d_{e} is transferred to the equivalent diameter $d_{\mathrm{e,eq}}$

$$d_{\mathrm{e,eq}} = d_{\mathrm{i}} + a_{\mathrm{iso}} \tag{23}$$

Substituting the proposed (22 and 23) into (19) obtains the modified stray capacitance for orthocyclic windings, as summarized in Fig. 7.

D. FEM and Experimental Verification: A Case Study

Prototypes L2/ 2o, L3/ 3o, L4/ 4o, L5/ 5o, and L8/ 8o are designed to verify the air gap compensation equations, as in Table III and Fig. 8. The inductors with winding II is in the normal group, while with IV is in the orthocyclic group.

Fig. 9 is the comparison for the L*i*o with compact orthocyclic windings. The parallel-plate model (17) considers the original definition of the inter-layer insulation distance a_{iso} in width direction (c.f. Fig. 1 and Fig. 2 (a.1)). Due to the compact winding structure, the built inductors are with negative value of original a_{iso}. So the calculated equivalent permittivity and the effective capacitance distance decrease, which finally leads to the decrease of the calculated capacitance. The original equation for the orthocyclic winding (19) without equivalent permittivity and diameter compensation equations (22, 23) neglects the inter-layer insulation distance a_{iso}, which overestimates the capacitance in all cases. It results in a maximum error of 111.5%. The proposed orthocyclic equation uses (19) and the compensation equations. It considers a_{iso} and obtains the lowest errors in all cases, with the maximum error 23.9%.

The wire position of built inductors is between the ideal type II and IV in reality. Therefore the measured values are also between the simulation results of those two type windings. However, from the comparison, it is more close to the simulated and calculated results of winding type IV.

V. Comparison of the Normal and Orthocyclic Windings

A. The Orthocyclic Resistance Ratio

The orthocyclic resistance ratio k_{r} is defined to compare the ac resistance ratio of orthocyclic winding $F_{\mathrm{r,o}}$ and the normal winding $F_{\mathrm{r,n}}$ with the same winding dimensions

$$k_{\mathrm{r}} = \frac{F_{\mathrm{r,o}}}{F_{\mathrm{r,n}}} \cdot 100\% \tag{24}$$

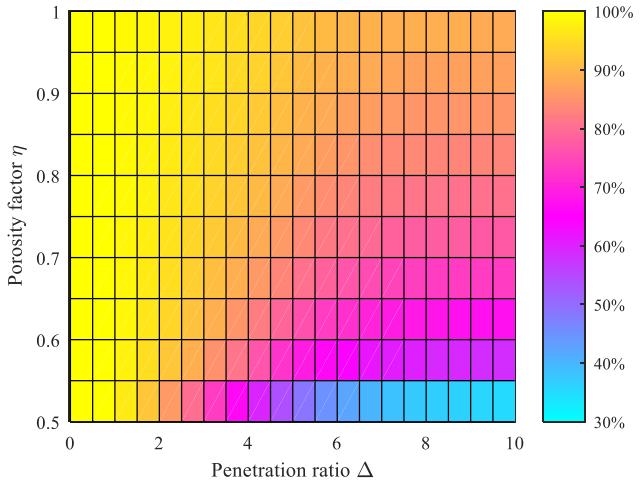

Fig. 10. The orthocyclic resistance ratio k_{r} with respect to the penetration ratio Δ and porosity factor η. The air gap between turns in adjutant layers $d_{\mathrm{air}} = 0$ in both windings. The number of layers $p = 5$, and the ratio map does not change significantly when p changes from 2 to 20.

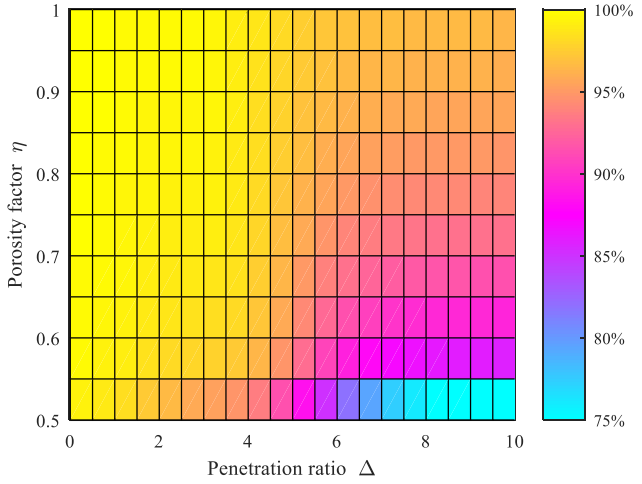

Fig. 11. The orthocyclic leakage inductance ratio k_{l} with respect to the penetration ratio Δ and porosity factor η. The air gap $d_{\mathrm{air}} = 0$ in both windings. The number of layers $p = 5$, however, the ratio map does not change significantly when p changes from 2 to 20. The radius ratio $k_{\mathrm{rad}} = 1.1$, and the $k_{\mathrm{l}} < 0.8$ area is $(\triangle > 6.0, \eta < 0.55)$. When $k_{\mathrm{rad}} = 2.0$, it changes to $(\triangle > 5.0, \eta < 0.55)$.

During comparison, the porosity factor η is assumed the same as the orthocyclic porosity factor η_{o}. Conclusions are obtained from the comparison in Fig. 10:

1) The ac resistance of the orthocyclic winding type IV is smaller compared with the normal winding type II.

2) The difference is neglectable when $(\triangle \leq 2.0, \eta \approx 1.0)$ where $k_{\mathrm{r}} > 90\%$. k_{r} decreases with the frequency f and the decrease of the porosity factor η, and is not relevant to the number of layers p.

3) $[k_{\mathrm{r}}]_{\mathrm{min}} = 35\%$ when $(\triangle = 10, \eta = 0.5)$.

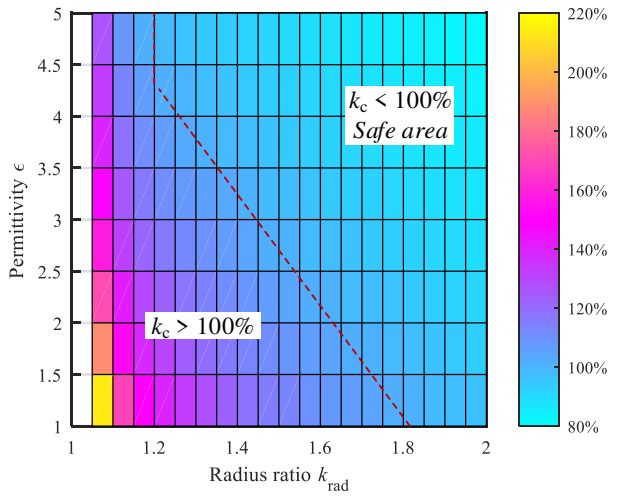

Fig. 12. The orthocyclic capacitance ratio k_c with respect to the permittivity ε_i and radius ratio k_{rad}. The air gap $d_{air} = 0$. The *safe area* is $k_c \leq 100\%$, which means the orthocyclic does not increase stray capacitance in this range.

B. The Orthocyclic Leakage Inductance Ratio

The orthocyclic leakage inductance ratio k_l is the ratio of the leakage inductance of the orthocyclic winding and normal winding and only considers the primary winding

$$k_l = \frac{\mu_0 p_1^2 \frac{l_w}{h_{w,o}} [d_{w1} \frac{p_1}{3} F_{L1,o} + d_{i1} \frac{(p_1-1)(2p_1-1)}{6p_1}]}{\mu_0 p_1^2 \frac{l_w}{h_{w,n}} [d_{w1} \frac{p_1}{3} F_{L1,n} + d_{i1} \frac{(p_1-1)(2p_1-1)}{6p_1}]} \cdot 100\% \quad (25)$$

where $h_{w,o}$, $h_{w,n}$ and $F_{L1,o}$, $F_{L1,n}$ are the equivalent winding height and leakage inductance ratio of orthocyclic and normal windings, respectively.

From the comparison in Fig. 11 it concludes (cont'd):

4) The leakage inductance of the winding type IV is smaller than type II.

5) The difference is negligible when $(\triangle \leq 5.0, \eta > 0.6)$ where $k_l > 90\%$. k_l decreases with the frequency f and the decrease of the porosity factor η, and is with no significant relevant to the number of layers p and radius ratio k_{rad}.

6) $[k_l]_{min} = 65\%$ when $(\triangle = 10, \eta = 0.5, k_{rad} = 2, p = 20)$.

C. The Orthocyclic Capacitance Ratio

The orthocyclic capacitance ratio k_c is to compare the layer capacitance of the orthocyclic and normal winding

$$k_c = \frac{C_{ww,o}}{C_{ww,n}} \cdot 100\% \quad (26)$$

k_c with ε_{wire} and k_{rad} is in Fig. 12 with conclusions (cont'd):

7) For the layer capacitance, the orthocyclic causes a maximum 118% increase or 20% decrease compared with the normal winding.

8) For the winding capacitance, this difference decreases with the increase of the number of layer p.

9) To ensure that the winding capacitance is not becoming larger when orthocyclic ($k_c \leq 100\%$), one method is to use large permittivity and thick insulation wire coating at the same time. The *safe area* for this is illustrated in the figure. Another method is to add insulation tapes between winding layers, which also leads to $k_r \approx 100\%$ and $k_l \approx 100\%$.

VI. Conclusions

In this paper, three parasitic formulas for orthocyclic windings are proposed, and differences between the orthocyclic and normal winding are systematically investigated. An orthocyclic coefficient is proposed for the ac resistance formula to modify the field distortion; it is also used in the leakage inductance model along with the new defined inter-layer distance; the modified stray capacitance model considers the air gap effect with compensating equations. The proposed formulas are verified by FEM simulation and experimental results with eight prototypes. They achieve higher accuracy compared with original models, especially with the increase of the frequency and air gap. The impact on the resistance, leakage inductance, and parasitic capacitance of orthocyclic windings with respect to normal windings in the presented case studies are summarized in Figs. 10 to 12.

References

[1] J. Biela and J. W. Kolar, "Using transformer parasitics for resonant converters-a review of the calculation of the stray capacitance of transformers," *IEEE Trans. Ind. Appl.*, vol. 44, no. 1, pp. 223–233, Jan. 2008.

[2] P. Thummala, H. Schneider, Z. Zhang, and M. A. E. Andersen, "Investigation of transformer winding architectures for high-voltage (2.5 kV) capacitor charging and discharging applications," *IEEE Trans. Power Electron.*, vol. 31, no. 8, pp. 5786–5796, Aug. 2016.

[3] J.-P. Vandelac and P. Ziogas, "A novel approach for minimizing high-frequency transformer copper losses," *IEEE Trans. Power Electron.*, vol. 3, no. 3, pp. 266–277, Jul. 1988.

[4] C. Sullivan, "Optimal choice for number of strands in a litz-wire transformer winding," *IEEE Trans. Power Electron.*, vol. 14, no. 2, pp. 283–291, Mar. 1999.

[5] R. De Doncker, D. Divan, and M. Kheraluwala, "A three-phase soft-switched high-power-density dc/dc converter for high-power applications," *IEEE Trans. Ind. Appl.*, vol. 27, no. 1, pp. 63–73, Jan. 1991.

[6] M. A. Bahmani and T. Thiringer, "Accurate evaluation of leakage inductance in high-frequency transformers using an improved frequency-dependent expression," *IEEE Trans. Power Electron.*, vol. 30, no. 10, pp. 5738–5745, Oct. 2015.

[7] Z. Ouyang, O. C. Thomsen, and M. A. E. Andersen, "Optimal design and tradeoff analysis of planar transformer in high-power dc-dc converters," *IEEE Trans. Ind. Electron.*, vol. 59, no. 7, pp. 2800–2810, Jul. 2012.

[8] M. A. Saket, N. Shafiei, and M. Ordonez, "LLC converters with planar transformers: Issues and mitigation," *IEEE Trans. Power Electron.*, vol. 32, no. 6, pp. 4524–4542, Jun. 2017.

[9] Z. Qin, Z. Shen, and F. Blaabjerg, "Modelling and analysis of the transformer current resonance in dual active bridge converters," in *Proc. IEEE ECCE*, Sep. 2017, pp. 4520–4524.

[10] P. Dowell, "Effects of eddy currents in transformer windings," *Proc. Inst. Electr. Eng.*, vol. 113, no. 8, pp. 1387–1394, Aug. 1966.

[11] W. Hurley, E. Gath, and J. Breslin, "Optimizing the AC resistance of multilayer transformer windings with arbitrary current waveforms," *IEEE Trans. Power Electron.*, vol. 15, no. 2, pp. 369–376, Mar. 2000.

[12] M. K. Kazimierczuk, *High-frequency magnetic components*. West Sussex, UK: John Wiley & Sons, 2009.

[13] M. Kaymak, Z. Shen, and R. W. D. Doncker, "Comparison of analytical methods for calculating the AC resistance and leakage inductance of medium-frequency transformers," in *Proc. IEEE Wksh. Contr. Modeling Power Electron.*, Jun. 2016, pp. 1–8.

[14] N. H. Kutkut, "A simple technique to evaluate winding losses including two-dimensional edge effects," *IEEE Trans. Power Electron.*, vol. 13, no. 5, pp. 950–958, Sep. 1998.

[15] A. Reatti and M. Kazimierczuk, "Comparison of various methods for calculating the AC resistance of inductors," *IEEE Trans. Magn.*, vol. 38, no. 3, pp. 1512–1518, May 2002.

[16] J. Ferreira, "Improved analytical modeling of conductive losses in magnetic components," *IEEE Trans. Power Electron.*, vol. 9, no. 1, pp. 127–131, Jan. 1994.

[17] R. Wojda and M. Kazimierczuk, "Analytical optimization of solid–round-wire windings," *IEEE Trans. Ind. Electron.*, vol. 60, no. 3, pp. 1033–1041, Mar. 2013.

[18] N. Wang, T. O'Donnell, and C. O'Mathuna, "An improved calculation of copper losses in integrated power inductors on silicon," *IEEE Trans. Power Electron.*, vol. 28, no. 8, pp. 3641–3647, Aug. 2013.

[19] X. Wang, L. Wang, L. Mao, and Y. Zhang, "Improved analytical calculation of high frequency winding losses in planar inductors," in *Proc. IEEE ECCE*, Sep. 2018, pp. 4336–4340.

[20] D. Whitman and M. K. Kazimierczuk, "An analytical correction to Dowell's equation for inductor and transformer winding losses using cylindrical coordinates," *IEEE Trans. Power Electron.*, vol. 34, no. 11, pp. 10 425–10 432, Nov. 2019.

[21] A. Ayachit and M. K. Kazimierczuk, "Thermal effects on inductor winding resistance at high frequencies," *IEEE Magn. Lett.*, vol. 4, p. 0 500 304, 2013.

[22] R. Wang, F. Xiao, Z. Zhao, Y. Shen, and G. Yang, "Effects of asymmetric coupling on winding AC resistance in medium-frequency high-power transformer," *IEEE Trans. Magn.*, vol. 50, no. 11, pp. 1–4, Nov. 2014.

[23] C. Feeney, J. Zhang, and M. Duffy, "Ac winding loss of phase-shifted coupled windings," *IEEE Trans. Power Electron.*, vol. 31, no. 2, pp. 1472–1478, 2015.

[24] E. Barrios, A. Ursua, L. Marroyo, and P. Sanchis, "Analytical design methodology for litz-wired high-frequency power transformers," *IEEE Trans. Ind. Electron.*, vol. 62, no. 4, pp. 2103–2113, Apr. 2015.

[25] R. P. Wojda and M. K. Kazimierczuk, "Winding resistance and power loss of inductors with litz and solid-round wires," *IEEE Trans. Ind. Appl.*, vol. 54, no. 4, pp. 3548–3557, 2018.

[26] C. Sullivan, "Computationally efficient winding loss calculation with multiple windings, arbitrary waveforms, and two-dimensional or three-dimensional field geometry," *IEEE Trans. Power Electron.*, vol. 16, no. 1, pp. 142–150, Jan. 2001.

[27] L. A. R. Tria, D. Zhang, and J. E. Fletcher, "High-frequency planar transformer parameter estimation," *IEEE Trans. Magn.*, vol. 51, no. 11, pp. 1–4, Nov. 2015.

[28] X. Nan and C. R. Sullivan, "An improved calculation of proximity-effect loss in high-frequency windings of round conductors," in *Proc. IEEE Power Electron. Spclst. Conf.*, vol. 2, Jun. 2003, pp. 853–860.

[29] M. Bahmani, T. Thiringer, and H. Ortega, "An accurate pseudoempirical model of winding loss calculation in HF foil and round conductors in switchmode magnetics," *IEEE Trans. Power Electron.*, vol. 29, no. 8, pp. 4231–4246, Aug. 2014.

[30] Y. Yin and L. Li, "Improved method to calculate the high-frequency eddy currents distribution and loss in windings composed of round conductors," *IET Power Electron.*, vol. 10, no. 12, pp. 1494–1503, 2017.

[31] N. Mohan, T. M. Undeland, and W. P. Robbins, *Power electronics: converters, applications, and design*. Hoboken, NJ, USA: John Wiley & Sons, 2007.

[32] Z. Ouyang, J. Zhang, and W. G. Hurley, "Calculation of leakage inductance for high-frequency transformers," *IEEE Trans. Power Electron.*, vol. 30, no. 10, pp. 5769–5775, Oct. 2015.

[33] W. G. Hurley and W. H. Wölfle, *Transformers and inductors for power electronics: theory, design and applications*. West Sussex, UK: John Wiley & Sons, 2013.

[34] K. Zhang, W. Chen, X. Cao, P. Pan, S. W. Azeem, G. Qiao, and F. Deng, "Accurate calculation and sensitivity analysis of leakage inductance of high-frequency transformer with litz wire winding," *IEEE Trans. Power Electron.*, vol. 35, no. 4, pp. 3951–3962, Apr. 2020.

[35] W. Tan, X. Margueron, L. Taylor, and N. Idir, "Leakage inductance analytical calculation for planar components with leakage layers," *IEEE Trans. Power Electron.*, vol. 31, no. 6, pp. 4462–4473, Jun. 2016.

[36] Z. Ouyang, W. G. Hurley, and M. A. E. Andersen, "Improved analysis and modeling of leakage inductance for planar transformers," *IEEE Trans. Emerg. Sel. Topics Power Electron.*, vol. 7, no. 4, pp. 2225–2231, Dec. 2019.

[37] J. Zhang, Z. Ouyang, M. C. Duffy, M. A. E. Andersen, and W. G. Hurley, "Leakage inductance calculation for planar transformers with a magnetic shunt," *IEEE Trans. Ind. Appl.*, vol. 50, no. 6, pp. 4107–4112, Nov. 2014.

[38] W. G. Hurley, M. C. Duffy, J. Zhang, I. Lope, B. Kunz, and W. H. Wölfle, "A unified approach to the calculation of self- and mutual-inductance for coaxial coils in air," *IEEE Trans. Power Electron.*, vol. 30, no. 11, pp. 6155–6162, Nov. 2015.

[39] F. Pan, L. Jin, P. Pan, and Z. Xu, "Design procedure of the leakage inductance for a pulse transformer considering winding structures," *IEEE Trans. Plasma Sci.*, vol. 45, no. 9, pp. 2504–2510, Sep. 2017.

[40] A. Stadler and M. Albach, "The influence of the winding layout on the core losses and the leakage inductance in high frequency transformers," *IEEE Trans. Magn.*, vol. 42, no. 4, pp. 735–738, 2006.

[41] H. Rossmanith and E. Stenglein, "Prediction of the leakage inductance in high frequency transformers," in *Proc. 18th Eur. Conf. Power Electron. Appl.*, Sep. 2016, pp. 1–10.

[42] M. Noah, T. Shirakawa, K. Umetani, J. Imaoka, M. Yamamoto, and E. Hiraki, "Effects of secondary leakage inductance on the LLC resonant converter," *IEEE Trans. Power Electron.*, vol. 35, no. 1, pp. 835–852, Jan. 2020.

[43] W. G. Hurley and D. J. Wilcox, "Calculation of leakage inductance in transformer windings," *IEEE Trans. Power Electron.*, vol. 9, no. 1, pp. 121–126, Jan. 1994.

[44] Z. Dong, R. Ren, B. Liu, and F. Wang, "Data-driven leakage inductance modeling of common mode chokes," in *Proc. IEEE ECCE*, Sep. 2019, pp. 6641–6646.

[45] M. Nazmunnahar, S. Simizu, P. R. Ohodnicki, S. Bhattacharya, and M. E. McHenry, "Finite-element analysis modeling of high-frequency single-phase transformers enabled by metal amorphous nanocomposites and calculation of leakage inductance for different winding topologies," *IEEE Trans. Magn.*, vol. 55, no. 7, pp. 1–11, Jul. 2019.

[46] A. Fouineau, M. Raulet, B. Lefebvre, N. Burais, and F. Sixdenier, "Semi-analytical methods for calculation of leakage inductance and frequency-dependent resistance of windings in transformers," *IEEE Trans. Magn.*, vol. 54, no. 10, pp. 1–10, Oct. 2018.

[47] M. Mogorovic and D. Dujic, "Medium frequency transformer leakage inductance modeling and experimental verification," in *Proc. IEEE ECCE*, Sep. 2017, pp. 419–424.

[48] S. Mohsenzade, M. Aghaei, and S. Kaboli, "Leakage inductance calculation of the transformers with disordered windings," *IEEE Trans. Plasma Sci.*, vol. 47, no. 4, pp. 1799–1807, Apr. 2019.

[49] M. Aghaei, S. Mohsenzade, and S. Kaboli, "On the calculation of the leakage inductance in transformers with nonideal windings," *IEEE Trans. Power Electron.*, vol. Early Access, 2020.

[50] Q. Yu and T. W. Holmes, "A study on stray capacitance modeling of inductors by using the finite element method," *IEEE Trans. Electromagn. Compat.*, vol. 43, no. 1, pp. 88–93, 2001.

[51] Z. D. Greve, O. Deblecker, and J. Lobry, "Numerical modeling of capacitive effects in HF multiwinding transformers-part II: Identification using the finite-element method," *IEEE Trans. Magn.*, vol. 49, no. 5, pp. 2021–2024, May 2013.

[52] H. Li and W. M. Rucker, "An accurate and efficient hybrid method for the calculation of the equivalent capacitance of an arbitrary-shaped coil," *IEEE Trans. Magn.*, vol. 52, no. 3, pp. 1–4, Mar. 2016.

[53] L. F. de Freitas Gutierres and G. C. Junior, "Analytical technique for evaluating stray capacitances in multiconductor systems: Single-layer air-core inductors," *IEEE Trans. Power Electron.*, vol. 33, no. 7, pp. 6147–6158, Jul. 2018.

[54] L. Dalessandro, F. da Silveira Cavalcante, and J. W. Kolar, "Self-capacitance of high-voltage transformers," *IEEE Trans. Power Electron.*, vol. 22, no. 5, pp. 2081–2092, Sep. 2007.

[55] M. Kovacic, Z. Hanic, S. Stipetic, S. Krishnamurthy, and D. Zarko, "Analytical wideband model of a common-mode choke," *IEEE Trans. Power Electron.*, vol. 27, no. 7, pp. 3173–3185, Jul. 2012.

[56] W. Tan, "Modeling and design of passive planar components for EMI filters," PhD thesis, Lille, France: Ecole Centrale de Lille, 2012.

[57] R. Chattopadhyay, M. A. Juds, P. R. Ohodnicki, and S. Bhattacharya, "Modelling, design and analysis of three limb high frequency transformer including transformer parasitics, for SiC mosfet based three port DAB," in *Proc. Annu. Conf. IEEE Ind. Electron. Soc.*, Oct. 2016, pp. 4181–4186.

[58] Z. Shen, H. Wang, Y. Shen, Z. Qin, and F. Blaabjerg, "An improved stray capacitance model for inductors," *IEEE Trans. Power Electron.*, vol. 34, no. 11, pp. 11 153–11 170, Nov. 2019.

[59] B. Liu, R. Ren, F. Wang, D. Costinett, and Z. Zhang, "Winding scheme with fractional layer for differential-mode toroidal inductor," *IEEE Trans. Ind. Electron.*, vol. 67, no. 2, pp. 1592–1604, Feb. 2020.

[60] E. Laveuve, J. P. Keradec, and M. Bensoam, "Electrostatic of wound components: Analytical results, simulation and experimental validation of the parasitic capacitance," in *Proc. Conf. IEEE Ind. Appl. Society Annu. Meeting*, Sep. 1991, 1469–1475 vol.2.

[61] X. Liu, Y. Wang, J. Zhu, Y. Guo, G. Lei, and C. Liu, "Calculation of capacitance in high-frequency transformer windings," *IEEE Trans. Magn.*, vol. 52, no. 7, pp. 1–4, Jul. 2016.
[62] K. Nguyen-Duy, Z. Ouyang, A. Knott, and M. A. E. Andersen, "Minimization of the transformer inter-winding parasitic capacitance for modular stacking power supply applications," in *Proc. Eur. Conf. Power Electron. Appl.*, Aug. 2014, pp. 1–10.
[63] F. Blache, J. P. Keradec, and B. Cogitore, "Stray capacitances of two winding transformers: Equivalent circuit, measurements, calculation and lowering," in *Proc. IEEE Ind. Appl. Soc. Ann. Meeting*, vol. 2, Oct. 1994, pp. 1211–1217.
[64] T. Duerbaum and G. Sauerlaender, "Energy based capacitance model for magnetic devices," in *Proc. IEEE APEC Exposit.*, Mar. 2001, pp. 109–115.
[65] D. Leuenberger and J. Biela, "Accurate and computationally efficient modeling of flyback transformer parasitics and their influence on converter losses," in *Proc. Eur. Conf. Power Electron. Appl.*, Sep. 2015, pp. 1–10.
[66] M. A. Saket, M. Ordonez, and N. Shafiei, "Planar transformers with near-zero common-mode noise for flyback and forward converters," *IEEE Trans. Power Electron.*, vol. 33, no. 2, pp. 1554–1571, Feb. 2018.
[67] Y. Li, H. Zhang, S. Wang, H. Sheng, C. P. Chng, and S. Lakshmikanthan, "Investigating switching transformers for common mode EMI reduction to remove common mode EMI filters and y-capacitors in flyback converters," *IEEE Trans. Emerg. Sel. Topics Power Electron.*, vol. 6, no. 4, pp. 2287–2301, Dec. 2018.
[68] P. Demumieux, O. Avino-Salvado, C. Buttay, C. Martin, F. Sixdenier, C. Joubert, J. S. Ngoua Teu Magambo, and T. Löher, "Design of a low-capacitance planar transformer for a 4 kW/500 kHz DAB converter," in *Proc. IEEE APEC Exposit.*, Mar. 2019, pp. 2659–2666.
[69] E. Snellinq, *SoftFerrites: Properties and Applications*. London, U.K.: Iliffe books Ltd, 1988.
[70] L. Deng, P. Wang, X. Li, H. Xiao, and T. Peng, "Investigation on the parasitic capacitance of high frequency and high voltage transformers of multi-section windings," *IEEE Access*, vol. 8, pp. 14 065–14 073, 2020.
[71] M. S. S. Nia, P. Shamsi, and M. Ferdowsi, "Investigation of various transformer topologies for HF isolation applications," *IEEE Trans. Plasma Sci.*, pp. 1–10, 2020.
[72] W. Schroder, "Berechnung der eigenschwingungen der doppellagigen langen spule," *Arch. Elektrotechnik*, vol. Band XI, Heft 6, pp. 203–229, 1922.
[73] M. Aghaei and S. Kaboli, "On the effect of disorder on stray capacitance of transformer winding in high-voltage power supplies," *IEEE Trans. Ind. Electron.*, vol. 64, no. 5, pp. 3608–3618, May 2017.
[74] J Koch, "Berechnung der kapazität von spulen, insbesondere in schalenkernen," *Valvo Berichte*, vol. 14, no. 3, pp. 99–119, 1968.
[75] A. Massarini and M. K. Kazimierczuk, "Self-capacitance of inductors," *IEEE Trans. Power Electron.*, vol. 12, no. 4, pp. 671–676, Jul. 1997.
[76] A. Massarini, "Analytical approach to the calculation of parasitic capacitance between winding turns," in *Proc. IEEE Int. Forum Res. Tech. Soc. Ind.*, Sep. 2018, pp. 1–4.
[77] Z. Shen, Y. Shen, Z. Qin, and H. Wang, "Modeling and optimization of displacement windings for transformers in dual active bridge converters," in *Proc. Int. Power Electronics Conf. (ECCE-Asia)*, May 2018, pp. 1925–1930.
[78] I. Villar, "Multiphysical characterization of medium-frequency power electronic transformers," PhD thesis, Lausanne, Switzerland: École Polytechnique Fédérale de Lausanne, 2010.
[79] H. Zuhrt, "Simple approximate formulas for the self capacitance of multi-layer coils," *Elekrotech. Zeitschrift*, vol. 55, pp. 662–665, Jul. 1934.

Zhan Shen (S'16) received the B.E. degree in electrical engineering and automation from Nanjing University of Aeronautics and Astronautics in 2013, and M.E. degree in electrical engineering from Southeast University in 2016, both in Nanjing, China. He is a Research Assistant at the Center of Reliable Power Electronics (CORPE), Aalborg University, Aalborg, Denmark. He was a Visiting Student and pursued his master thesis at the RWTH Aachen University, Aachen, Germany, from Oct. 2014 to Feb. 2016, and a Visiting Scholar with the Massachusetts Institute of Technology (MIT), Cambridge, MA, USA, from Oct. 2018 to Jan. 2019.

He was with the ABB Corporate Research Center, Beijing, China, in 2016. His research interests include the electromagnetic-thermal-reliability modeling and design of magnetic components in power electronic converters.

Huai Wang (M'12, SM'17) received the B.E. degree in electrical engineering, from Huazhong University of Science and Technology, Wuhan, China, in 2007 and the Ph.D. degree in power electronics, from the City University of Hong Kong, Hong Kong, in 2012. He is currently Professor with the Center of Reliable Power Electronics (CORPE), Department of Energy Technology at Aalborg University, Denmark. He was a Visiting Scientist with the ETH Zurich, Switzerland, from Aug. to Sep. 2014, and with the Massachusetts Institute of Technology (MIT), USA, from Sep. to Nov. 2013. He was with the ABB Corporate Research Center, Switzerland, in 2009. His research addresses the fundamental challenges in modelling and validation of power electronic component failure mechanisms, and application issues in system-level predictability, condition monitoring, circuit architecture, and robustness design.

Dr. Wang received the Richard M. Bass Outstanding Young Power Electronics Engineer Award from the IEEE Power Electronics Society in 2016, and the Green Talents Award from the German Federal Ministry of Education and Research in 2014. He is currently the Chair of IEEE PELS/IAS/IES Chapter in Denmark. He serves as an Associate Editor of IET Electronics Letters, IEEE JOURNAL OF EMERGING AND SELECTED TOPICS IN POWER ELECTRONICS, and IEEE TRANSACTIONS ON POWER ELECTRONICS.